A Quantitative Study on the Photothermal Effect of Immuno Gold Nanocages Targeted to Breast Cancer Cells

Leslie Au[†], **Desheng Zheng**[‡], **Fei Zhou**[§], **Zhi-Yuan Li**[§], **Xingde Li**[‡], and **Younan Xia**[∥],[*]

[†]Department of Chemistry, University of Washington, Seattle, Washington 98195

[‡]Department of Bioengineering, University of Washington, Seattle, Washington 98195

[§]Institute of Physics, Chinese Academy of Sciences, Beijing 100080, PR China

[∥]Department of Biomedical Engineering, Washington University, St. Louis, Missouri 63130

Abstract

Gold nanocages with an average edge length of 65 ± 7 nm and a strong absorption peak at 800 nm were conjugated with monoclonal antibodies (anti-HER2) to target breast cancer cells (SK-BR-3) through the epidermal growth factor receptor (in this case, HER2), which is overexpressed on the surfaces of the cells. Both the number of immuno Au nanocages immobilized per cell and the photothermal therapeutic effect were quantified using flow cytometry. The targeted cells were irradiated with a pulsed near-infrared laser, and by varying the power density, the duration of laser exposure, and the time of response after irradiation, we were able to optimize the treatment conditions to achieve effective destruction of the cancer cells. We found that cells targeted with the immuno Au nanocages responded immediately to laser irradiation and that the cellular damage was irreversible at power densities greater than $1.6 \ W/cm^2$. The percentage of dead cells increased with increasing exposure time up to 5 min and then became steady. By quantifying the photothermal effect of immuno Au nanocages, critical information with regards to both the optimal dosage of nanocages and parameters of the laser irradiation has been garnered and will be applied to future *in vivo* studies.

Keywords

gold nanocages; surface plasmon resonance; photothermal effect; targeted cancer therapy; bioconjugation

Owing to their biocompatibility and tunable light absorption/scattering properties, gold nanostructures have recently been demonstrated for use in various biomedical applications.[1–3] The well-established surface chemistry for gold also allows one to target specific cells by attaching different moieties (*e.g.*, antibodies, peptides, and DNAs) to the nanostructures. As demonstrated in a number of studies, the strong optical absorption of some Au nanostructures makes them attractive as photothermal agents for cancer therapy.[4] Unlike the conventional methods for cancer treatment (*e.g.*, surgical removal, radiotherapy, and chemotherapy), photothermal treatment—in which light is converted to heat *in vivo* to kill cells *via* hyperthermia—holds promise as a noninvasive technique for the selective destruction of cancer cells with minimal injury to the surrounding healthy cells. Several types of Au nanostructures with strong optical absorption in the near-infrared region (where blood and soft tissue are essentially transparent) have been developed; among these are Au nanoshells supported on

*Address correspondence to E-mail: xia@biomed.wustl.edu .

silica cores,[5,6] Au nanorods,[7–9] and Au nanocages (*i.e.*, hollow structures with porous walls). [10,11] Calculations based upon the discrete dipole approximation (DDA) method indicate that the nanoshells tend to scatter light predominately, whereas both the nanorods and nanocages are stronger light absorbers.[1] Although the ratio of light absorption to scattering may vary slightly with the dimensions of the nanostructures, these calculations suggest that the nanocages and nanorods are more effective optical absorbers than nanoshells. The large absorption cross section of the Au nanocages was recently confirmed experimentally by optical coherent tomography (OCT) measurements and found to be approximately 5 orders of magnitude greater than that of the conventional organic dyes.[12] Finally, we have found that the absorption peaks of nanocages can be more conveniently and precisely fine-tuned than those of other Au nanostructures, potentially allowing for their large-scale production for practical applications.[13,14]

The photothermal effects of the various Au nanostructures were recently demonstrated, and all were shown qualitatively to be able to destroy targeted cancer cells upon irradiation with a near-infrared laser.[15–19] However, there are no quantitative studies of the cellular damage in which parameters such as the number of immobilized Au nanostructures per cell, the waiting time after irradiation, and the duration of laser exposure were considered. In this Article, we quantify the photothermal effect of immuno Au nanocages (*i.e.*, nanocages conjugated with anti-HER2 monoclonal antibodies) targeted to SK-BR-3 cells—a well-characterized breast cancer cell line that overexpresses the epidermal growth factor receptor 2 (EGFR2 or HER2) —by employing flow cytometry. In doing so, we were able to better elucidate the interactions between the nanocages, cells, and laser, which will contribute to the optimization of treatment parameters for future *in vivo* experiments.

RESULTS AND DISCUSSION

Synthesis and Characterization of the Immuno Au Nanocages

For this study, Au nanocages of 65 ± 7 nm in edge length and 7.5 ± 1 nm in wall thickness were synthesized through a galvanic replacement reaction using silver nanocubes (~54 nm in edge length) as the sacrificial template and chloroauric acid, $HAuCl_4$, as the precursor to Au. [10–14]Figure 1A shows scanning electron microscopy (SEM) and transmission electron microscopy (TEM) images of the Au nanocages. These Au nanocages were shown to contain 37% residual Ag in the form of an alloy with Au by energy dispersive X-ray analysis. If necessary, the residual Ag can be selectively removed through a dealloying process with the use of $Fe(NO_3)_3$ or NH_4OH.[20] Using the DDA method, the absorption, scattering, and extinction spectra were calculated for a Au nanocage with an edge length of 65 nm, a wall thickness of 7.5 nm, and a pore diameter of 20 nm at the corners. The results are shown in Figure 1B. The C_{abs} and C_{sca} were found to be peaked at 6.16×10^{-14} and 2.02×10^{-14} m^2, respectively, with a C_{abs}/C_{sca} ratio of ~3.0. The measured extinction spectrum of the nanocages shown in the inset is consistent with the calculation. The discrepancy in peak width can be ascribed to the variations in edge length, wall thickness, the degree of corner truncation, and the porosity for the Au nanocages contained in a bulk sample. The Au nanocages were then conjugated to anti-HER2 antibodies using a two-step procedure.[21,22] After conjugation, the extinction peak of these immuno Au nanocages slightly red-shifted from 800 to 805 nm, which was expected due to the small change of refractive index on the surface of the nanocages. It is worth pointing out that this small shift can be taken into account during the preparation of the pristine Au nanocages to ensure that there will be an exact overlap between the resonance peak of the immuno Au nanocages and the central wavelength of the laser. Recently, Au nanocages with similar optical properties were demonstrated by us to be effective agents for the *in vitro* photothermal destruction of cancer cells.[19] Thus, it was reasoned that these immuno Au nanocages would work well for the quantitative studies described here.

Quantification of the Targeting Process *In Vitro*

Previously, the targeting selectivity of our bioconjugation protocol was demonstrated by immunofluorescence imaging and SEM.[21,22] However, no information with regards to the number of nanocages attached to the cell surface was obtained. This information is important as it can tell us the amount of nanocages necessary to induce a photothermal therapeutic effect and allow for better comparisons between our nanocages and other nanostructures. Thus, in the first part of this study, we sought to quantify the average number of Au nanocages attached per cell. In addition to Au nanocages, Au nanospheres of 40 nm in diameter were used as a reference to validate the experimental procedure due to their well-defined size, shape, and composition. As a first approximation, SEM images were taken of the SK-BR-3 cells treated with immuno Au nanocages or nanospheres. The number of nanostructures observed in a randomly selected $2\,\mu m \times 1.5\,\mu m$ portion of the cell was counted from multiple samples. Upon the basis of the number of nanostructures measured in that section and the dimensions of the cell as revealed by SEM imaging, the surface coverage was estimated to be approximately 200–2000 Au nanostructures per cell. This broad range could be attributed to the inhomogeneous distribution of receptors on the cell surface.[23] Panels A and B of Figure 2 show SEM images of individual cells that had been targeted with the immuno Au nanospheres and nanocages, respectively. Interestingly, TEM imaging of a microtomed sample revealed that the Au nanocages were not solely immobilized on the surface of the cell. As Figure 2C shows, some of them were internalized into the cell, although none appeared to enter the nucleus. The HER2 antibodies have been reported to trigger endocytosis, but the exact mechanism for nanocage uptake has yet to be elucidated.[24,25]

While electron microscopy allows us to see where the immuno Au nanostructures are located (on the surface *vs* inside) and roughly at what coverage, this technique is of rather limited power when dealing with large numbers of cells. To more accurately quantify the targeting efficiency of the immuno Au nanostructures, we decided to use flow cytometry coupled with inductively coupled plasma mass spectroscopy (ICP-MS). With this approach, the amount of Au contained in a specific number of cells can be determined. Then, from the geometric parameters of the nanostructures, the number of nanostructures per cell can be calculated. Specifically, the amount of Au can be easily determined by analyzing the sample with ICP-MS, while the number of cells in the sample can be easily quantified by spiking it with a known amount of Sphero Ultra Rainbow beads, followed by flow cytometry counting. Figure 2D shows a typical flow cytometry graph where forward scatter (*x*-axis) and right angle scatter (*y*-axis) can be used to differentiate the size difference between the beads and the cells. Then the number of cells can be quantified using FCS Express software to gate the populations of both cells and beads. For the standard *in vitro* targeting procedure described in the Experimental Methods, we found that there were approximately 460 ± 130 Au nanospheres per cell and roughly 400 ± 90 Au nanocages per cell; both numbers fall within the initial estimates from SEM images. In future *in vivo* studies, this information should allow for the administration of immuno Au nanocages in proper dosages to induce a photothermal effect for tumors of known sizes.

Quantification of the Photothermal Treatment Process *In Vitro*

The photothermal treatment with the immuno Au nanocages was implemented *in vitro* with SK-BR-3 cells. The central wavelength of the radiation was 805 nm with a bandwidth of 54 nm, so there was an optimal overlap with the absorption peak of the immuno Au nanocages. Yet, good spectral overlap between the light source and the light absorbing nanostructure will not alone ensure a good therapeutic effect. Factors such as time of cellular response to laser irradiation, laser power density, and time of laser exposure could also influence the efficiency of the photothermal effect. Thus, we systematically varied these parameters and quantified the amount of cellular death under each condition using flow cytometry coupled with propidium iodide (PI) staining.

PI is a popular nuclear or chromosomal counterstain in multicolor fluorescence techniques and is commonly used in flow cytometry to differentiate cell cycles. When PI binds to DNA by intercalating between the bases, it fluoresces about 20–30-fold stronger than unbound PI.[26] Since PI is not permeable to live cells, it works well as a marker to quantify the number of dying or dead cells in a sample. In addition, it only requires a short incubation time (<15 min) and can generate well-separated populations of live and dead/dying cells. In a typical flow cytometry measurement, one can use PI fluorescent and forward scattering signals to quantify the cellular death caused by the photothermal effect.

Figure 3A shows the experimental setup, where cells in the center of a well (6.38 mm in diameter; 96-well plate) were irradiated with the Ti:sapphire laser with a spot size of 2 mm. The SK-BR-3 cells are adherent, hence their position is fixed on the surface of the well. It should be pointed out that the laser only irradiated 9.8% of the cells in each well (note cells are not drawn to scale). We also tried to use smaller wells (*e.g.*, 3.7 mm in diameter; 384-well plate), but they were found to increase the experimental error, so the 96-well plate was used. In one study, the treated cells were harvested at various times after irradiation to investigate when cells start to respond to the photothermal treatment. In Figure 3B, the cells were irradiated at a laser power density of 4.77 W/cm^2 for 5 min. After that, the cells were returned to a 37 ° C incubator for a specific duration of time before the percentage of cellular damage was quantified. Cells targeted with the immuno Au nanocages (●) exhibited more cellular damage at early harvest times. The cellular damage decreased at harvest times greater than 3 h after laser exposure, which could possibly be attributed to (*i*) the cells untouched by the laser proliferated during their course in the incubator, resulting in a dilution of the destructed cells, and/or (*ii*) some of the damaged cells recovered from the photothermal effect. Cells irradiated under the same conditions but without the immuno Au nanocages (○) exhibited no significant response during the given time. A small, unavoidable percentage of cellular death was observed, probably due to the pipetting and handling of cells during sample preparation. The results of this study indicate that the cells respond immediately to the photothermal treatment and should be harvested within 3 h after irradiation to better reflect the treatment. Harvest times shorter than 1 h after laser irradiation are not feasible due to the time required to prepare the sample for flow cytometry.

Panels C and D of Figure 3 show the flow cytometry graphs of the cells with and without targeting by the immuno Au nanocages, respectively, at a harvest time of 3 h after laser irradiation. Forward scatter is plotted on the *x*-axis, and PI emission signal is plotted on the *y*-axis. The flow cytometry graphs were sectioned into four quadrants. Quadrant I, exhibiting a large forward scattering and low PI signal, represents the population of live cells. Since the live cells have intact cell membranes, PI could not stain their DNAs. Quadrant II, displaying large forward scattering and high PI signal, corresponds to the population of dying cells. The membranes of these cells had been compromised so PI could penetrate and then hybridize with their DNAs. The population of dead cells, or stained DNAs, exhibits a high PI and small forward scattering signal as shown in quadrant III. These are free DNAs, no longer enclosed within a membrane. Quadrant IV reveals a population with small forward scattering and low PI signal that could be attributed to instrumental background signals and debris from ruptured cells. The population in quadrant IV does not representatively correspond to live or damaged cells, so the percentage of cellular damage was normalized to the population in quadrants I, II, and III. A higher population of damage was observed when the cells were targeted with the immuno Au nanocages. These results exemplify that the immuno Au nanocages are effective photothermal agents capable of absorbing light and converting it into heat. The flow cytometry data also reveal that cells targeted by the immuno Au nanocages display irreversible damage upon photothermal treatment, as shown by the larger population in quadrant III, where the cellular membrane is broken to such an extent that the cell can no longer function nor recover from the damage. Although a small portion of damaged cells are present in quadrant II, the

majority is observed in quadrant III, suggesting that the decrease of cellular damage over time was caused by the proliferation of cells outside the spot size and not by the recovery of the compromised cells as speculated earlier.

We also investigated the effect of the laser power density. Figure 4 shows a plot of cellular damage against the laser power density for cells irradiated for 5 min and harvested 3 h after irradiation. In the control, the cells without Au nanocages (◯) maintained viability and the values are consistent with the control experiments shown in Figure 3. Cells treated with the immuno Au nanocages (●) exhibited little or no damage at power densities less than 1.6 W/cm^2. At some threshold between 1.6 and 2.4 W/cm^2, the damage becomes significantly greater than the control. At power densities greater than 1.6 W/cm^2, the damage for cells treated with the immuno Au nanocages increases linearly, similar to what was found in our previous publication.[19] As the power density increased to 6.4 W/cm^2, the cellular damage increased to 55%. Since the laser irradiated only 9.8% of the well, the cellular damage extended beyond the spot size of the laser, as is expected because the amount of heat generated increases with increasing laser power. As will be discussed later, the heat generated within the spot size can transfer to surrounding regions. Depending on the stage and type of cancer, cancerous cells can invade local regions of tumor sites and removal of nearby regions may be necessary, thus this linear relationship provides a means of calibrating the treatment to kill cancerous cells that have broken away from the primary tumor. Alternatively, by keeping the power density low, collateral damage to nearby healthy cells can be minimized.

The cells were also exposed to the laser for different periods of time. Figure 5 shows a plot of cellular damage against the duration of laser exposure for cells irradiated at 4.77 W/cm^2 and harvested 3 h after irradiation. In the control, cells without immuno Au nanocage treatment (◯) maintained viability, which is consistent with the results from the control experiments shown in Figure 3 and Figure 4. The percentage of damage for cells treated with immuno Au nanocages (●) continuously increased for the first 5 min. After 5 min, the cellular death reached a steady percentage at about 35%. An exposure time of 1 min resulted in cellular damage (18%) larger than the percentage of cells irradiated by the laser (9.8%), suggesting that Au nanocages in the spot size of the laser irradiation responded quickly to the exposure. As the exposure time increased to 5 min, the cellular death increased, signifying that the death outside the spot size of the laser depends on the amount of time necessary for heat generated from the immuno Au nanocages to transfer to cells outside the irradiated regions. The cellular death becomes steady after 5 min, which could be attributed to other temperature gradients in the surroundings, thus establishing equilibrium. This relationship is important for calibrating the laser parameters for practical applications of *in vivo* photothermal treatment. For example, a highpowered laser can be expensive, so rather than increasing the power of the laser, the time of laser exposure could be easily prolonged; however, after some extended period of time, the cellular death will become steady. This parameter provides another approach to treat the local invasion of tumor.

CONCLUSION

In summary, we have quantified the targeting and photothermal therapeutic effects of 65 nm immuno Au nanocages on SK-BR-3 breast cancer cells. Additionally, by combining PI fluorescent labeling with flow cytometry, we are able to distinguish between live and dead cells. This technique proved to be extremely powerful at determining and quantifying the number of nanocages per cell. The relationship between laser parameters (*i.e.*, power density and duration of laser exposure) and cellular damage was also better elucidated. The information garnered from this work will aid in future *in vivo* studies in which the dosage of immuno Au nanocages and the power density and exposure time of the laser can be optimized to treat individual conditions (*e.g.*, tumor size and local invasion of tumor). Additionally, this study provided more information about the interaction between the cells, immuno Au nanocages,

and laser. For example, it was previously unknown that the immuno Au nanocages were internalized by the cells. Our photothermal studies also showed that cells targeted with immuno Au nanocages respond immediately to the laser stimuli, and that the amount of cellular death can be controlled by both the exposure time and power density of the laser. Cells treated under the same experimental conditions but without immuno Au nanocages maintained their viability. The efficacy for the immuno Au nanocages to kill cancer cells can be attributed to their selective targeting and large absorption cross section of near-infrared light. The results reported here provide insight into how the photothermal response of immuno Au nanocages can be optimized and controlled. This knowledge is critical to providing effective, noninvasive treatment of cancer *in vivo via* photothermal therapy. Future work will also address the stability of Au nanocages in conjunction with its biodistribution *via* local and systemic administration as well as collateral damage to nearby healthy cells.

EXPERIMENTAL METHODS

Synthesis of Au Nanocages

Au nanocages were prepared using the galvanic replacement reaction between $HAuCl_4$ and Ag nanocubes as the template. The detailed procedure has been reported in our previous publications.[10,11,14] Briefly, 500 µL of the Ag nanocubes (~3 nM) was added to 5 mL of deionized water containing poly(vinyl pyrrolidone) (PVP, 1 mg mL^{-1}, MW ≈ 55 000, Aldrich, 856568) hosted in a 50 mL flask under magnetic stirring and then heated to boil for 10 min. In the meantime, an aqueous solution of $HAuCl_4$ (0.5 mM, Aldrich, 520918) was prepared. The $HAuCl_4$ was added to the flask *via* syringe pump (KDS-200, Stoelting, Wood Dale, IL) at a rate of 45 mL h^{-1} until the solution had an optical extinction peak at 800 nm as confirmed by UV–vis spectroscopy (Agilent 8453). The solution was refluxed for another 30 min until the color of the reaction was stable. Once cooled to room temperature, the sample was centrifuged and washed with saturated NaCl solution to remove AgCl and with water several times to remove PVP and NaCl before characterization by SEM and TEM.

Synthesis of Ag Nanocubes

The Ag nanocubes were prepared using the sulfide-mediated polyol process as described in previous publications.[13,14] In a typical synthesis, 6 mL of ethylene glycol (EG, J.T. Baker, 9300–03) was preheated to 155 °C for 1 h under magnetic stirring. EG solutions containing Na_2S (3 mM, Aldrich, 208043), PVP (0.18 M as calculated in terms of the repeating unit), and $AgNO_3$ (0.28 M, Aldrich, 209139) were prepared. The Na_2S solution (80 µL) was injected into the hot EG, followed by the PVP solution (1.5 mL) and then the $AgNO_3$ solution (0.5 mL). The reaction underwent color changes from yellow to reddish brown to opaque green-gray with plating on the vial walls. The reaction was completed within 20 min. The reaction solution was diluted with acetone, and the product was isolated by centrifugation. The product was washed twice with deionized water then collected by centrifugation at 13 000 rpm for 5 min and redispersed by brief sonication in deionized water (4 mL).

Preparation of Immuno Au Nanocages

The Au nanocages were functionalized using a two-step protocol reported in previous publications[21,22] in order to target SK-BR-3 cells. In the first step, the Au nanocages (2 nM, 1 mL) were incubated with an aqueous solution of the thiolated poly(ethylene glycol) (PEG) OPSS-PEG-SC (1 mM, 1 mL, Layson Bio, MW ≈ 5000) at room temperature in the dark for ~12 h. Excess OPSS-PEG-SC was removed from the nanocages by discarding the supernatant after centrifugal separation. The sample was then washed once with Dulbecco's phosphate buffer solution (PBS, 1×, Invitrogen, 14190), centrifuged at 10 000 rpm for 10 min, and redispersed in PBS. In the second step, the PEGylated Au nanocages were incubated with monoclonal anti-HER2 (Invitrogen, 28-0003Z) in PBS overnight at 4 °C. The sample was then

centrifuged for 5 min at 10 000 rpm to remove excess antibodies and redispersed in 1 mL of PBS. The final products are referred throughout the paper as immuno Au nanocages and could be stored at 4 °C for up to 1 week.

Cell Culture

The breast cancer cell line SK-BR-3 (ATCC, HTB-30) was cultured in McCoy's 5a Medium Modified (ATCC, 30–2007) containing 10% fetal bovine serum (FBS, Invitrogen, 16000) and 5% streptomycin/penicillin (Invitrogen, 15140) at 37 °C in 5% CO_2 (v/v). The medium was changed 2–3 times a week. When they reached a confluency of 60–90%, the adherent cells were removed from the growth vessel with trypsin (Gibco, 25200). The trypsin was deactivated by adding the growth medium. The suspension of cells was centrifuged for 5 min at 1000 rpm, and the pellet of cells was resuspended in growth medium and then transferred to a desired growth vessel (flask, multiwell plate, or Petri dish) for quantitative and photothermal studies.

Preparation and Imaging of SEM Samples

The SK-BR-3 cells were transferred to a silicon wafer and allowed to settle overnight in a 12-well plate. The SK-BR-3 cells were fixed with methanol and then washed three times with Tris-buffered saline Tween-20 (TBST), followed by a rinse with Tris-buffered saline (TBS). The cells were incubated with 20 μL of the immuno Au nanocages in TBS for at least 3 h, with 1 h of gentle agitation. After that, the cells were washed three times with TBST and one time with TBS. The sample was briefly rinsed with water and dried before SEM characterization using a Sirion XL field-emission microscope (FEI, Hillsboro, OR) operated at 5 kV.

Preparation and Imaging of Microtomed Samples

The SK-BR-3 cells were grown in a 35 mm Petri dish. They were then incubated with 50 μL of the immuno Au nanocages in medium for 3 h, with 1 h of gentle agitation. Then, the cells were rinsed three times with PBS and fixed with a solution containing glutaraldehyde (2.5%), cacodylate (0.1 M), sucrase (0.1 M), and $CaCl_2$ (0.4 mM) overnight at 4 °C. The cells were post-fixed with OsO_4 (1%) in cacodylate (0.1 M) and $CaCl_2$ (0.4 mM) for 2 h at room temperature, followed by uranyl acetate (2%) in water for 1 h at room temperature. The cells were dehydrated through a graded ethanol series and finally embedded in eponate (Ted Pella, Redding, CA) epoxy resin and set aside to polymerize for 48 h at 60–65 °C. A microtome (Reichert/Jung Ultracut E, Leica, Arcadia, CA) equipped with a diamond knife was used to cut the cured epoxy resin into slices with a thickness of 80–100 nm. The cell slices were contrasted with an aqueous solution of uranyl acetate (7%) and lead citrate.[27] The samples were examined using a JEOL EXIII TEM.

Quantification of the Number of Au Nanostructures Attached per Cell

SK-BR-3 cells were grown in a 12-well plate and incubated with 20 μL of the immuno Au nanospheres (Ted Pella, 40 nm in diameter) or 20 μL of the immuno Au nanocages for 3 h (with 1 h of gentle agitation) in a solution that contained the growth medium. They were rinsed three times with PBS. The adherent cells were removed from the growth vessel with trypsin as described previously. The suspension of cells was collected and spiked with a known amount of Sphero Ultra Rainbow beads (Spherotech, URFP-100-2, 10.2 μm). A known amount of the sample was then inserted into an influx flow cytometer (Cytopeia) with a 488 nm argon laser as the excitation source. Data analysis was performed using FCS Express (DeNovo) software to determine the number of cells in the solution. The remainder of the sample was analyzed to determine the amount of Au present in the sample using ICP-MS (PerkinElmer Elan DRC-e).

Photothermal Treatment

SK-BR-3 cells in 96-well plates were incubated with 12 µL of the immuno Au nanocages for 3 h (with 1 h of gentle agitation). The cells in the center of the wells were irradiated with a Ti:sapphire laser with a central wavelength at 805 nm and a bandwidth of 54 nm. The near-infrared light source was a femtosecond pulsed irradiation generated from a homebuilt Kerr-lens mode-locked Ti:sapphire laser with 82 MHz repetition rate. The Gaussian beam size was adjusted with a convex lens (B coating, BK7, $f = 75$ mm), and the sample was positioned at a distance such that the spot size was 2 mm in diameter. An iris diaphragm was used to block light outside the spot. The laser power density was adjusted using a neutral attenuator. The duration of irradiation and the power density for photothermal treatment are described in the text. After laser irradiation, the cells were incubated in the medium at 37 °C until they were harvested and analyzed.

Quantification of the Photothermal Effect

After a certain period of incubation (as indicated in the text), the cells were rinsed with PBS and then harvested with trypsin as described previously. The suspension of cells and rinses with PBS were collected in a tube for flow cytometry analysis. The cellular suspension (400 µL) was treated with PI (12 µL, Molecular Probes, 1 µg/mL stock, in dH_2O) and then inserted into the flow cytometer. The PI fluorescent signal was collected using a 625/25 BP filter. The data were analyzed using the FCS Express software.

Acknowledgment

REFERENCES AND NOTES

1. Hu M, Chen J, Li ZY, Au L, Hartland GV, Li X, Marquez M, Xia Y. Gold Nanostructures: Engineering Their Plasmonic Properties for Biomedical Applications. Chem. Soc. Rev 2006;35:1084–1094. [PubMed: 17057837]

2. Xia Y, Halas NJ. Shape-Controlled Synthesis and Surface Plasmonic Properties of Metallic Nanostructures. MRS Bull 2005;30:338–348.

3. Jain PK, Huang X, El-Sayed I, El-Sayed M. Noble Metals on the Nanoscale: Optical and Photothermal Properties and Some Applications in Imaging, Sensing, Biology, and Medicine. Acc. Chem. Res. 2008in press

4. Pissuwan D, Valenzuela SM, Cortie MB. Therapeutic Possibilities of Plasmonically Heated Gold Nanoparticles. Trends Biotechnol 2006;24:62–67. [PubMed: 16380179]

5. Oldenberg SJ, Averitt RD, Westcott SL, Halas NJ. Nanoengineering of Optical Resonances. Chem. Phys. Lett 1998;28:243–247.

6. Averitt RD, Westcott SL, Halas NJ. Linear Optical Properties of Gold Nanoshells. J. Opt. Soc. Am. B 1999;16:1824–1832.

7. Link S, El-Sayed MA. Spectral Properties and Relaxation Dynamics of Surface Plasmon Electronic Oscillations in Gold and Silver Nanodots and Nanorods. J. Phys. Chem. B 1999;103:8410–8426.

8. Murphy CJ, Sau TK, Gole AM, Orendorff CJ, Gao J, Gou L, Hunyadi SE, Li T. Anisotropic Metal Nanoparticles: Synthesis, Assembly, and Optical Applications. J. Phys. Chem. B 2005;109:13857–13870. [PubMed: 16852739]

9. Kelly KL, Coronado E, Zhao LL, Schatz GC. The Optical Properties of Metal Nanoparticles: The Influence of Size, Shape, and Dielectric Environment. J. Phys. Chem. B 2003;107:668–677.

10. Sun Y, Xia Y. Shape-Controlled Synthesis of Gold and Silver Nanoparticles. Science 2002;298:2176–2179. [PubMed: 12481134]

11. Sun Y, Xia Y. Mechanistic Study on the Replacement Reaction between Silver Nanostructures and Chloroauric Acid in Aqueous Medium. J. Am. Chem. Soc 2004;126:3892–3901. [PubMed: 15038743]

12. Cang H, Sun T, Li ZY, Chen JY, Wiley BJ, Xia YN, Li XD. Gold Nanocages as Contrast Agents for Spectroscopic Optical Coherence Tomography. Opt. Lett 2005;30:3048–3050. [PubMed: 16315717]

13. Siekkinen AR, McLellan JM, Chen J, Xia Y. Rapid Synthesis of Small Silver Nanocubes by Mediating Polyol Reduction with a Trace Amount of Sodium Sulfide or Sodium Hydrosulfide. Chem. Phys. Lett 2006;432:491–496. [PubMed: 18496589]

14. Skrabalak SE, Au L, Li X, Xia Y. Facile Synthesis of Ag Nanocubes and Au Nanocages. Nat. Protocols 2007;2:2182–2190.

15. Loo C, Lowery A, Halas N, West J, Drezek R. Immunotargeted Nanoshells for Integrated Cancer Imaging and Therapy. Nano Lett 2005;5:709–711. [PubMed: 15826113]

16. O'Neal DP, Hirsch LR, Halas NJ, Payne JD, West JL. Photo-Thermal Tumor Ablation in Mice Using Near Infrared-Absorbing Nanoparticles. Cancer Lett 2004;209:171–176. [PubMed: 15159019]

17. Hirsch LR, Stafford RJ, Bankson JA, Sershen SR, Rivera B, Price RE, Hazle JD, Halas NJ, West JL. Nanoshell-Mediated Near-Infrared Thermal Therapy of Tumors under Magnetic Resonance Guidance. Proc. Natl. Acad. Sci. U.S.A 2003;23:13549–13554. [PubMed: 14597719]

18. Huang X, El-Sayed IH, Qian W, El-Sayed MA. Cancer Cell Imaging and Photothermal Therapy in the Near-Infrared Region by Using Gold Nanorods. J. Am. Chem. Soc 2006;128:2115–2120. [PubMed: 16464114]

19. Chen J, Wang D, Xi J, Au L, Siekkinen A, Warsen A, Li Z-Y, Zhang H, Xia Y, Li XD. Immuno Gold Nanocages with Tailored Optical Properties for Targeted Photothermal Destruction of Cancer Cells. Nano Lett 2007;7:1318–1322. [PubMed: 17430005]

20. Lu X, Au L, McLellan J, Li ZY, Marquez M, Xia Y. Fabrication of Cubic Nanocages and Nanoframes by Dealloying Au/Ag Alloy Nanoboxes with an Aqueous Etchant Based on $Fe(NO_3)_3$ or NH_4OH. Nano. Lett 2007;7:1764–1769. [PubMed: 17489641]

21. Chen J, Saeki F, Wiley B, Cang H, Cobb MJ, Li Z-Y, Au L, Zhang H, Kimmey MB, Li X, et al. Gold Nanocages: Bioconjugation and Their Potential Use as Optical Imaging Contrast Agents. Nano Lett 2005;5:473–477. [PubMed: 15755097]

22. Chen J, Wiley B, Li Z, Cang H, Campbell D, Saeki F, Au L, Lee J, Li X, Xia Y. Gold Nanocages: Engineering Their Structure for Biomedical Applications. Adv. Mater 2005;17:2255–2261.

23. Nagy P, Jenei A, Kirsch AK, Szollosi J, Damjanovich S. Activation-Dependent Clustering of the ErbB2 Receptor Tyrosine Kinase Detected by Scanning Near-Field Optical Microscopy. J. Cell Sci 1999;112:1733–1741. [PubMed: 10318765]

24. Frankel A. New HER2-Directed Therapies for Breast Cancer. Clin. Cancer Res 2002;8:1699–1701. [PubMed: 12060606]

25. Hurwitz E, Stancovski I, Sela M, Yarden Y. Suppression and Promotion of Tumor Growth by Monoclonal Antibodies to ErbB-2 Differentially Correlate with Cellular Uptake. Proc. Natl. Acad. Sci. U.S.A 1995;92:3353–3357. [PubMed: 7724565]

26. Arndt-Jovin DJ, Jovin TM. Fluorescence Labeling and Microscopy of DNA. Methods Cell. Biol 1989;30:417–448. [PubMed: 2467179]

27. Reynolds ES. The Use of Lead Citrate at High pH as an Electron-Opaque Stain in Electron Microscopy. J. Cell Biol 1963;16:208–212. [PubMed: 13986422]
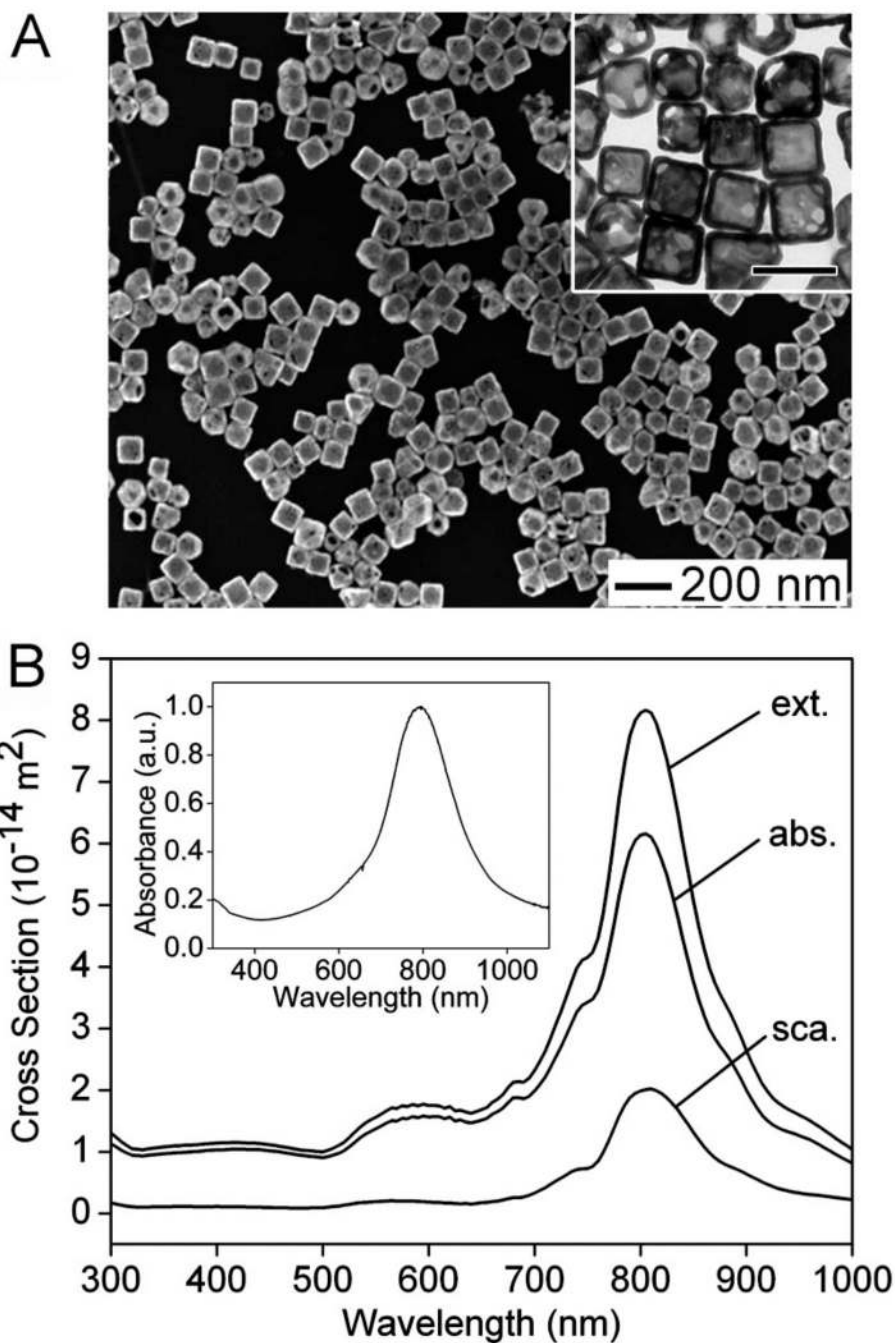
Figure 1.
(A) SEM and TEM (inset) images of Au nanocages synthesized using the galvanic replacement reaction in which Ag nanocubes serve as a sacrificial template. The scale bar in the inset represents 100 nm. (B) The absorption (C_{abs}), scattering (C_{sca}), and extinction (C_{ext}) cross sections (note that $C_{ext} = C_{abs} + C_{sca}$) as a function of wavelength were calculated using the DDA method for a Au nanocage with the following geometrical parameters: edge length = 65 nm, wall thickness = 7.5 nm, and corner holes with diameter = 20 nm. Also for the DDA calculations, the nanocages were assumed to be in water and have a composition of 37% Ag and 63% Au. The inset shows the UV–visible absorbance spectrum for the nanocages shown in (A), which have a resonance peak at 800 nm, in agreement with the calculations.
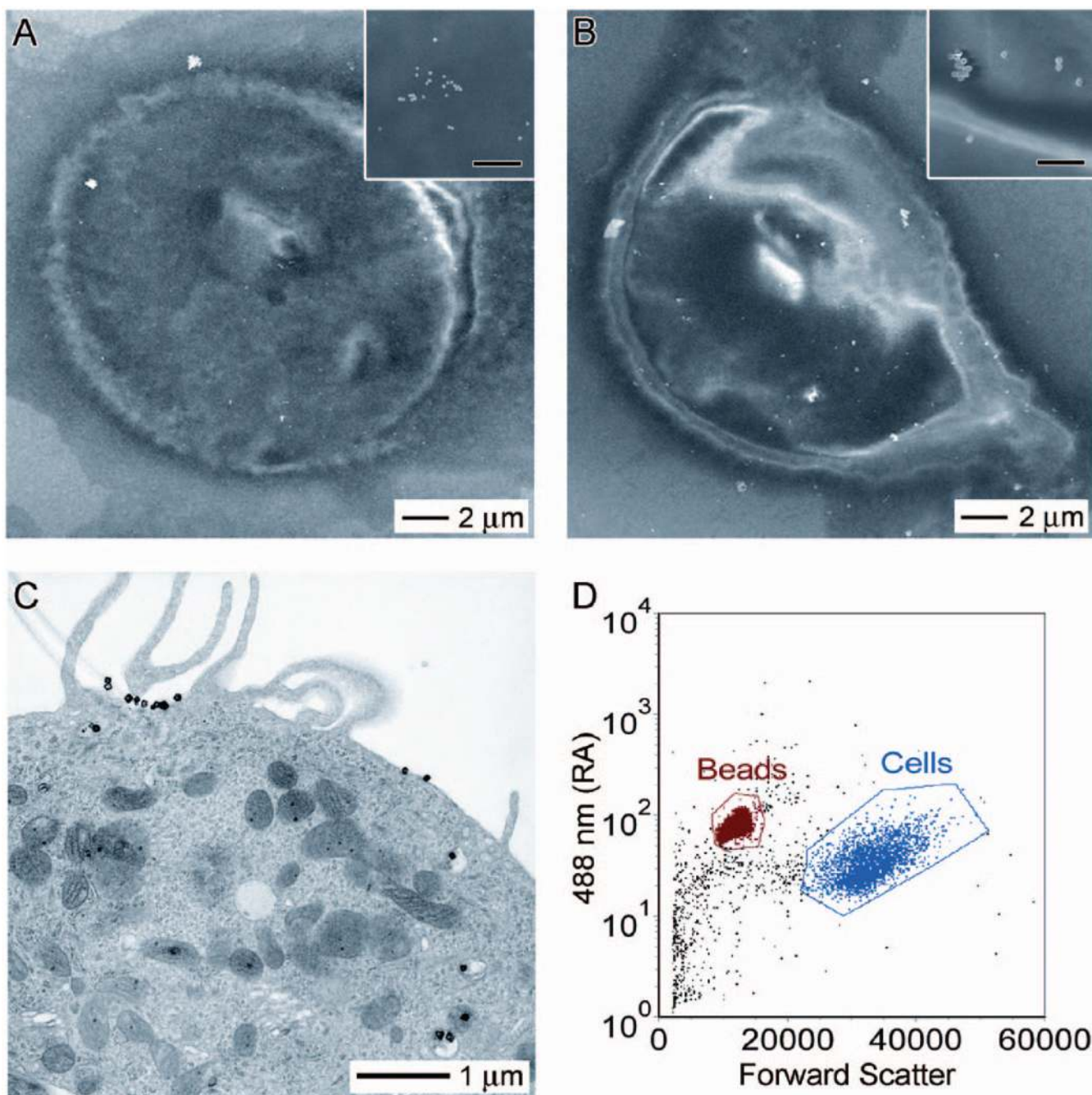
Figure 2.
SEM images of SK-BR-3 cells targeted with immuno Au nanospheres (A) and nanocages (B). SEM images at higher magnification (insets) reveal that the bright spots in the SEM images are indeed nanospheres and nanocages, respectively. The scale bar in the insets represents 500 nm. (C) TEM image of a microtomed SK-BR-3 cell conjugated with immuno Au nanocages. In addition to immuno Au nanocages decorating the surface of the cell, this microtomed TEM image reveals that some immuno Au nanocages are internalized by the cell. However, they do not appear to enter the nucleus. (D) Typical flow cytometry graph indicating how the forward scatter (*x*-axis) and right angle scatter (*y*-axis) can be used to differentiate the size difference between beads and cells. As the concentration of beads is known for a given sample, it provides

an internal reference for measuring the concentration of cells; when these data are coupled with ICP-MS analysis for Au, the number of immuno Au nanocages per cell can be estimated.
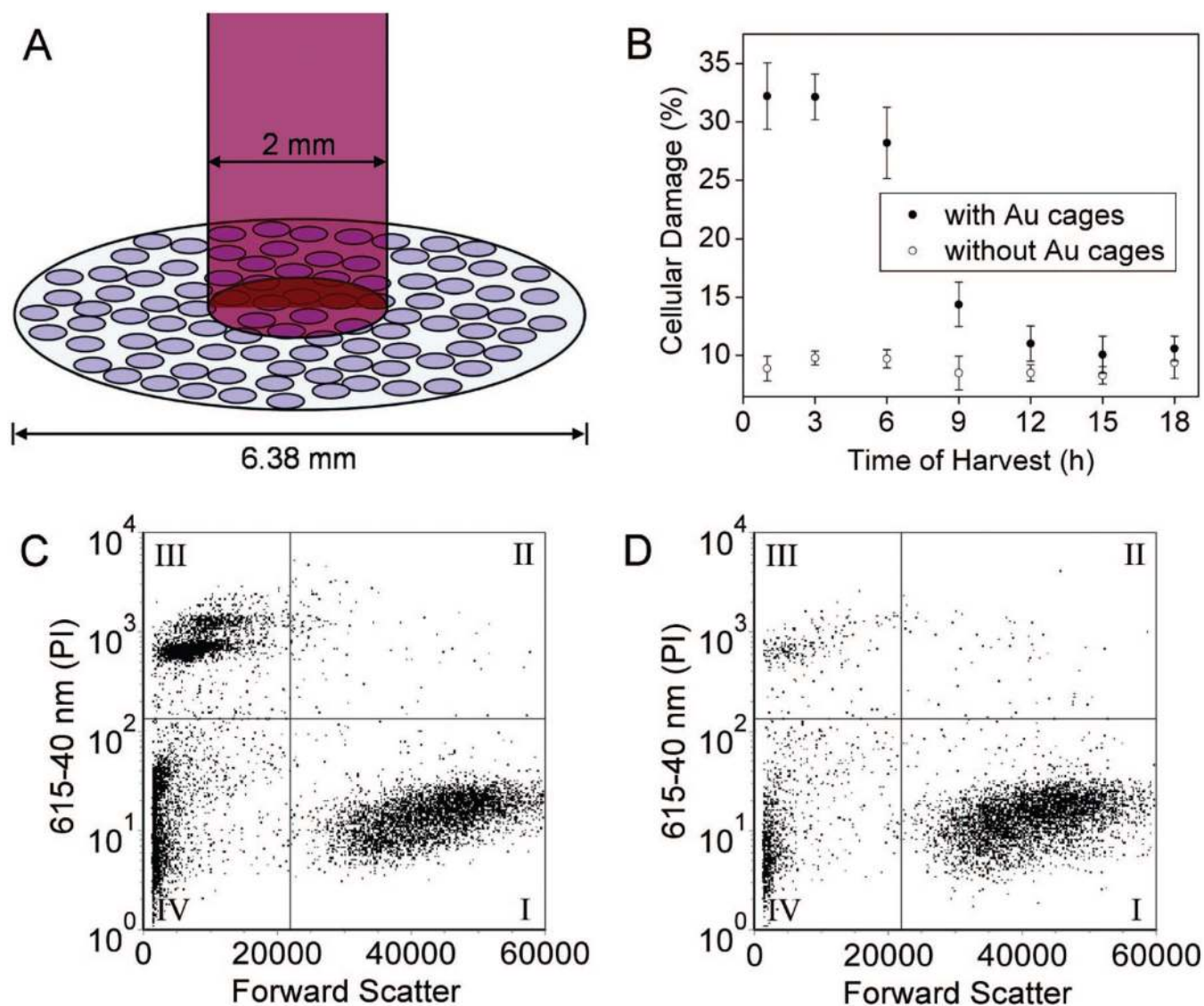
Figure 3.
(A) Illustration depicting the experimental setup used for photothermal therapy of SK-BR-3 cells. The cellular growth vessel had a diameter of 6.38 mm. The cells were irradiated with an 805 nm Ti:sapphire laser with a spot size of 2 mm. Thus, only 9.8% of the cells in the well were exposed to the laser. Note: cells not drawn to scale. (B) Plots of the percentage of cellular damage *versus* harvest time when SK-BR-3 cells were irradiated for 5 min at a laser power of 4.77 W/cm^2: ●, results for cells targeted with immuno Au nanocages; ○, control (no incubation with immuno Au nanocages). (C) The flow cytometry graph analyzed to determine the percentage of cellular death after SK-BR-3 cells were incubated with immuno Au nanocages, irradiated for 5 min at a power density of 4.77 W/cm^2, then harvested at 3 h for analysis. (D) Flow cytometry graph obtained from the control experiment in which SK-BR-3 cells were not treated with immuno Au nanocages but treated to similar laser treatment. For both (C) and (D), the signal in quadrant III corresponds to population of dead cells.
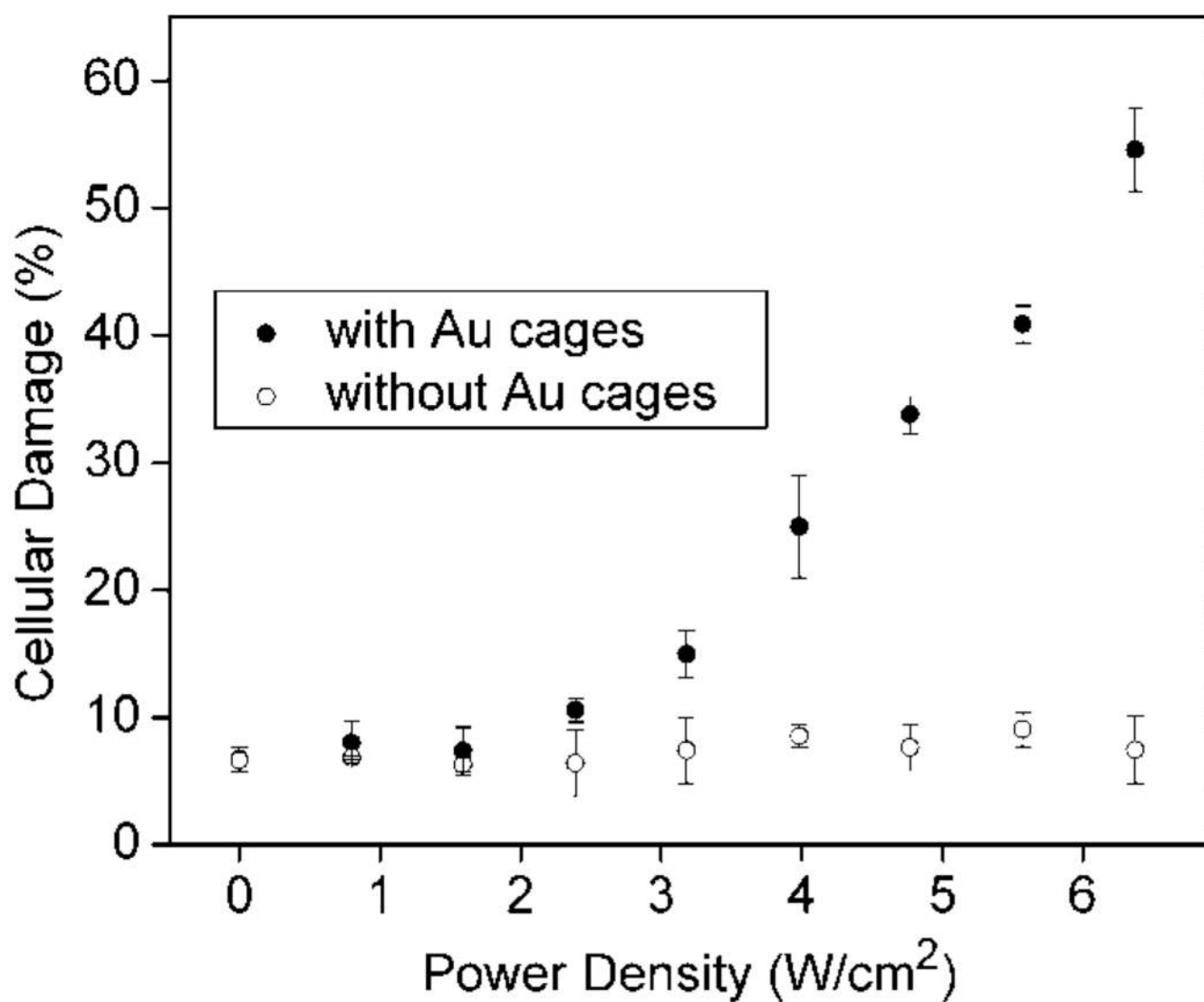
Figure 4.
Plots of cellular damage *versus* laser power density for SK-BR-3 cells incubated with immuno
Au nanocages (●) and for the control in which cells were not incubated with immuno Au
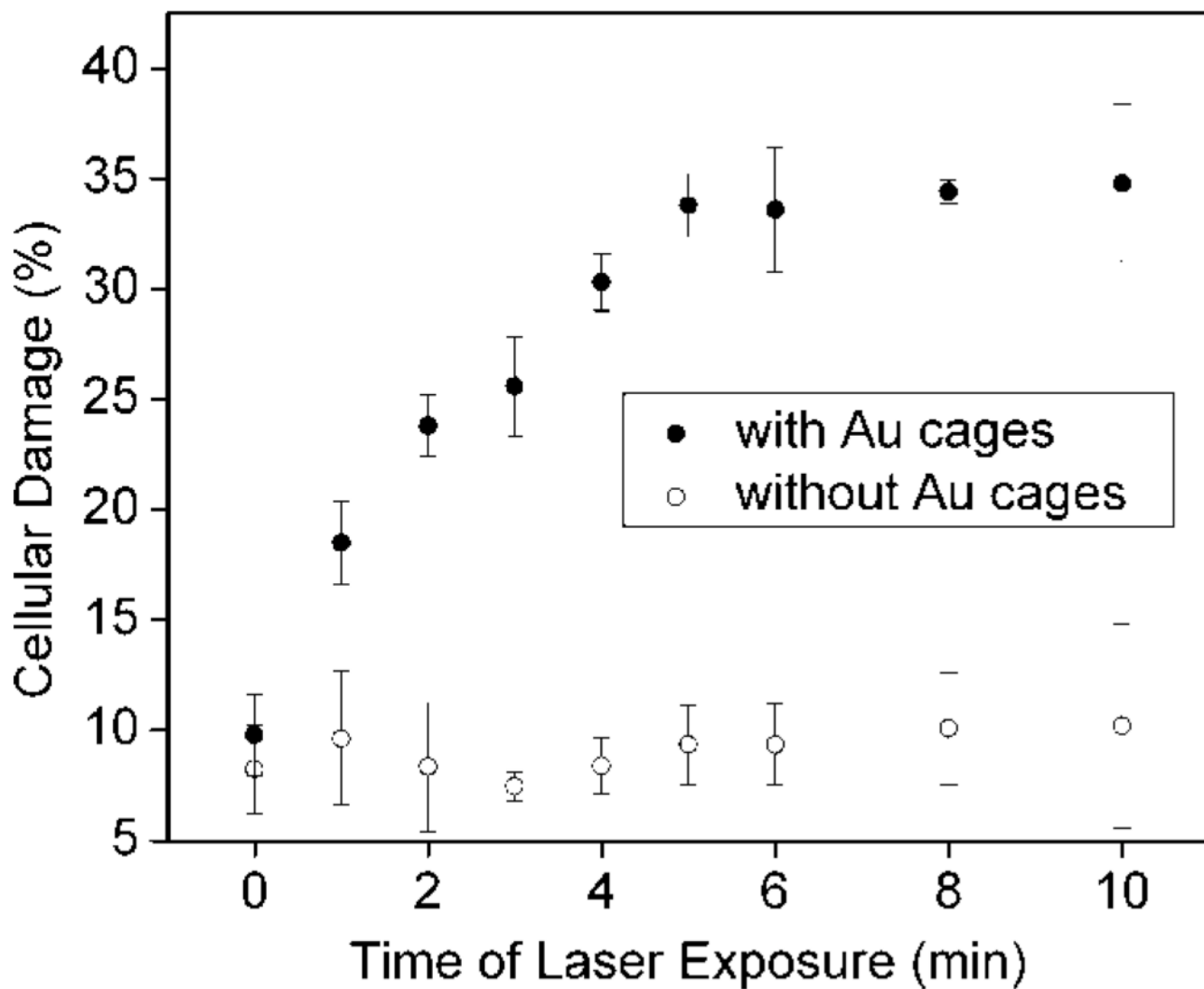nanocages (◯). Cells were irradiated for 5 min and harvested for analysis 3 h after irradiation.

Figure 5.
Plots of cellular damage *versus* laser exposure time for SK-BR-3 cells incubated with immuno Au nanocages (●) and for the control in which cells were not incubated with immuno Au nanocages (○). In both cases, the cells were irradiated with a 805 nm laser at a power density of 4.77 W/cm^2 then harvested for analysis 3 h after irradiation.